Role of helical structure and dynamics in oligoadenylate synthetase 1 (OAS1) mismatch tolerance and activation by short dsRNAs

Samantha L. Schwartz[a,b], Debayan Dey[a], Julia Tanquary[a,b], Camden R. Bair[c], Anice C. Lowen[c], and Graeme L. Conn[a,b,1]

[a]Department of Biochemistry, Emory University School of Medicine, Atlanta, GA 30322; [b]Graduate Program in Biochemistry, Cell and Developmental Biology, Graduate Division of Biological and Biomedical Sciences, Emory University, Atlanta, GA 30322; and [c]Department of Microbiology and Immunology, Emory University School of Medicine, Atlanta, GA 30322

Edited by Joseph Puglisi, Department of Structural Biology, Stanford University School of Medicine, Stanford, CA; received May 23, 2021; accepted November 17, 2021

The 2′-5′-oligoadenylate synthetases (OAS) are innate immune sensors of cytosolic double-stranded RNA (dsRNA) that play a critical role in limiting viral infection. How these proteins are able to avoid aberrant activation by cellular RNAs is not fully understood, but adenosine-to-inosine (A-to-I) editing has been proposed to limit accumulation of endogenous RNAs that might otherwise cause stimulation of the OAS/RNase L pathway. Here, we aim to uncover whether and how such sequence modifications can restrict the ability of short, defined dsRNAs to activate the single-domain form of OAS, OAS1. Unexpectedly, we find that all tested inosine-containing dsRNAs have an increased capacity to activate OAS1, whether in a destabilizing (I•U) or standard Watson–Crick-like base pairing (I–C) context. Additional variants with strongly destabilizing A•C mismatches or stabilizing G–C pairs also exhibit increased capacity to activate OAS1, eliminating helical stability as a factor in the relative ability of the dsRNAs to activate OAS1. Using thermal difference spectra and molecular dynamics simulations, we identify both increased helical dynamics and specific local changes in helical structure as important factors in the capacity of short dsRNAs to activate OAS1. These helical features may facilitate more ready adoption of the distorted OAS1-bound conformation or stabilize important structures to predispose the dsRNA for optimal binding and activation of OAS1. These studies thus reveal the molecular basis for the greater capacity of some short dsRNAs to activate OAS1 in a sequence-independent manner.

OAS/RNase L | innate immunity | double-stranded RNA | structure/dynamics | inosine

The 2′-5′-oligoadenylate synthetase (OAS) family of nucleotidyl transferases are responsible for detecting double-stranded RNA (dsRNA), a potent pathogen-associated molecular pattern, typically absent in the uninfected cell but abundant during viral infection. The dsRNA binding promotes structural rearrangements necessary to form the OAS active site for synthesis of 2′-5′ phosphodiester-linked oligoadenylate (2-5A) signaling molecules (1, 2), which, in turn, promote dimerization and activation of latent endoribonuclease (RNase L) (3–5). Activated RNase L restricts viral infection by degrading viral and cellular RNA, including ribosomal RNA (rRNA), transfer RNA, and specific messenger RNA transcripts required for cell growth, proliferation, and differentiation (6–10).

The human OAS family comprises three catalytically active members: OAS1, OAS2, and OAS3, which possess one, two, and three OAS domains, respectively. In each enzyme, only one domain retains 2-5A synthesis activity (11–13). Additional OAS domains are speculated to be responsible for expanding the dsRNA binding surface to allow detection of a wider range of dsRNA lengths. As such, OAS1 is capable of detecting short dsRNAs (>18 base pairs), although it is also activated by longer dsRNAs, while OAS3 requires >50 base pairs (1, 13, 14).

While the OAS/RNase L pathway is most notable for restricting viral replication and spread of infection, important roles in limiting other infectious diseases, for example, tuberculosis (15, 16) and malaria (17), have more recently emerged. There is also a growing appreciation for potential role(s) of OAS in the context of normal cell function in the absence of infection, as suggested by association of defects in the OAS/RNase L pathway and diseases such as autoimmune disorders (18–21) and cancer (22, 23). Further, OAS1, in particular, has been directly linked to resistance for the only approved treatment for gastric cancer (24). Despite these advances, we still do not fully understand how OAS1 avoids unwanted self-activation by cellular RNAs containing double-stranded regions or how specific features within a dsRNA, of viral or cellular origin, combine to promote OAS1 activity.

Recent studies have suggested that the cellular adenosine-to-inosine (A-to-I) editing enzyme adenosine deaminase acting on RNA (ADAR1) may play a protective role against self-activation of the OAS/RNase L pathway and other innate immune sensors of dsRNA (25–27). *ADAR1* mutations cause Aicardi–Goutières syndrome (AGS), an autoimmune disorder associated with the up-regulation of interferon (IFN)-stimulated genes (28), identifying ADAR1 as a suppressor of Type I IFN

Significance

The innate immune system is a collection of essential frontline defenses against infectious pathogens such as viruses. Currently, however, we do not fully understand how one innate immune sensor of double-stranded RNA (dsRNA), oligoadenylate synthetase 1 (OAS1), is regulated in the absence of infection, nor the specific features of dsRNA molecules that lead to potent OAS1 activation. Here, we uncover a molecular basis for how sequence-independent features of short dsRNAs influence the extent of OAS1 activation. We also find that OAS1 is able to sense inosine-containing dsRNAs, suggesting that RNA editing may not be a protective mechanism to avoid aberrant cellular activation of OAS1 as has been proposed for other dsRNA sensing innate immune proteins.

Author contributions: S.L.S., D.D., A.C.L., and G.L.C. designed research; S.L.S., D.D., J.T., and C.R.B. performed research; S.L.S., D.D., A.C.L., and G.L.C. analyzed data; S.L.S. and G.L.C. wrote the paper; and S.L.S., D.D., J.T., C.R.B., A.C.L., and G.L.C. edited and reviewed the final manuscript.

The authors declare no competing interest.

This article is a PNAS Direct Submission.

This article is distributed under Creative Commons Attribution-NonCommercial-NoDerivatives License 4.0 (CC BY-NC-ND).

[1]To whom correspondence may be addressed. Email: gconn@emory.edu.

This article contains supporting information online at http://www.pnas.org/lookup/suppl/doi:10.1073/pnas.2107111119/-/DCSupplemental.

Published January 11, 2022.

signaling. In mice, deletion of *Adar1* is embryonic lethal but can be rescued by mutations in other genes involved in IFN induction, and a corresponding human cell–lethal phenotype can be reversed by mutation of *RNASEL* (29). These findings indicate that the absence of ADAR1 editing leads to an accumulation of cellular RNAs with the capacity to activate the OAS/RNase L pathway. A-to-I editing is proposed to destabilize dsRNA regions within cellular RNAs, thus providing an essential mechanism by which their propensity to inadvertently activate OAS proteins (and other dsRNA sensors) is reduced (25–27). However, to date, whether or not OAS1 or other OAS family members are activated by A-to-I edited cellular dsRNAs has yet to be directly tested.

Similarly, several studies have identified molecular signatures, including nucleotide sequences and structural motifs, responsible for potentiating OAS1 activation in vitro and in human cells (30–33), but their mechanism of action is not well understood. Previously, it was thought that OAS1 required only two key determinants for activation: 1) perfectly double-stranded RNA that 2) meets the length requirements needed to span the entire dsRNA binding surface (>18 bp). The crystal structure of dsRNA-bound human OAS1 contained an 18-bp dsRNA (Fig. 1*A*) with two overlapping, antiparallel copies of a previously identified OAS1 activation consensus sequence WWN_9WG, where W is A or U and N is any nucleotide (1, 31). The structure revealed the partially conserved (WW/WG) nucleotides of one of these WWN_9WG motifs to be positioned on the same face of the RNA helix, allowing their minor groove base pair edges to mediate key contacts with OAS1 residues. The relative lack of contacts between OAS1 and the central region of the consensus (i.e., "N_9") suggested that, consistent with its variable sequence, this intervening region's main function was simply to serve as the necessary spacer to ensure the WW/WG dinucleotides were positioned appropriately (31). However, our recent work with variants of the 18-bp dsRNA revealed that changes in the N_9 sequence also have the propensity to strongly influence the extent of OAS1 activation (34). The OAS1-bound dsRNA is distorted from a canonical A-form helix, adopting a bent conformation to make direct contacts with OAS1 at each end of the RNA helix (1). N_9 sequences with greater inherent flexibility or that are in some other way more predisposed to adopt the required bent conformation might offer a plausible explanation for increased activation without specific sequence requirement or need for direct interaction with OAS1. Indeed, during the course of the present work, a molecular dynamics (MD) study revealed the propensity for an AU tract in dsRNAs to induce helical bending (35). Such an AU tract, of the minimum 3-nt length to induce bending, is present in the 18-bp dsRNA immediately preceding the conserved G nucleotide of the consensus sequence engaged by OAS1 (Fig. 1*A*).

We began this work to address whether and how OAS1 activation is reduced by A-to-I "editing" in the context of a short dsRNA. More broadly, we aimed to assess the role of helical structure and flexibility in OAS1 activation and whether such properties might underpin the observed influence of the consensus N_9 region on OAS1 activation. We find that A-to-I substitutions within the N_9 region reduce dsRNA stability as anticipated but, contrary to expectation, do not ablate OAS1 activation. Rather, distinct sequence changes in the consensus N_9 region enhance OAS1 activation by either increasing overall helical dynamics or stabilizing specific local features of helical structure in a sequence-independent manner.

Results

A-to-I "Editing" Does Not Prevent OAS1 Activation. To test the effect of A-to-I editing on OAS1 activation in the context of a short defined dsRNA, we generated variants of the RNA

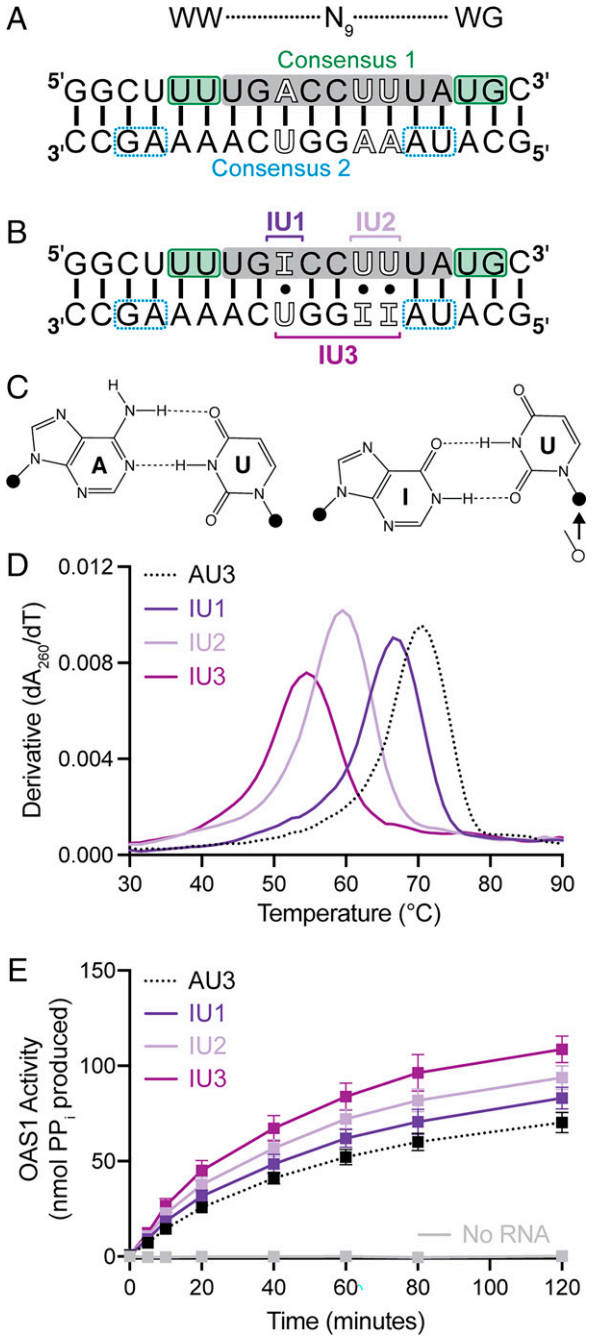

Fig. 1. Central I•U base pairs do not diminish OAS1 activation by short dsRNA. (*A*) Schematic of the 18-bp dsRNA with two overlapping, antiparallel WWN_9WG OAS1 activation consensus sequences (conserved WW/WG nucleotides, green and blue, respectively). Nonconserved (N_9, gray) nucleotides are only highlighted for the "top" strand which is engaged by OAS1 in the OAS1–dsRNA crystal structure (1). The A–U base pairs selected to generate dsRNA variants for these studies are indicated in outline font. (*B*) Three inosine-containing dsRNAs were generated by introducing one (IU1), two (IU2), or three (IU3; combined IU1 and IU2) A-to-I substitutions. (*C*) Comparison of canonical Watson–Crick A–U (*Left*) and noncanonical I•U (*Right*) base pairing, noting a shift in base and phosphodiester backbone positions necessary to maintain two hydrogen-bonding interactions (open and closed circles with arrow). (*D*) UV thermal melting profiles (shown for the 100-mM NaCl condition) indicate that I•U containing dsRNAs (purple shades) are progressively destabilized (lower T_m) with increasing number of changes compared to the AU3 dsRNA (black dotted line). (*E*) Reaction progress curves from an in vitro chromogenic assay of OAS1 activity using a single dsRNA concentration (300 nM) with the same dsRNAs showing OAS1 activation is concomitantly enhanced as the number of I•U base pairs increases.

construct used in the human OAS1–dsRNA crystal structure (1) and our previous analyses of OAS1 activation (32, 34). As these prior studies showed that OAS1 engages productively with only one of the two OAS1 activation consensus sequences in this dsRNA (highlighted green in Fig. 1*A*), we focused on the intervening N_9 region within this "top" strand consensus. Three A–U base pairs were selected for A-to-I editing following the considerations that changes should not be immediately adjacent to the conserved WW/WG top-strand consensus nucleotides nor directly alter the conserved nucleotides of the "bottom" strand consensus. Thus, any changes in OAS1 activation should arise due to alterations in helical structure within the central region of the dsRNA, which is not directly contacted by OAS1, and not because of alterations to important interactions with the conserved consensus residues.

We generated three inosine-containing 18-bp dsRNAs by making one (IU1), two (IU2), or three (IU3; combined IU1 and IU2) I•U changes at A–U base pairs in the center of the "parent" 18-bp dsRNA (Fig. 1 *B* and *C* and *SI Appendix*, Fig. S1), hereafter referred to as "AU3" for consistency in naming of these dsRNAs. To maintain hydrogen bonding, I•U base pairs have altered backbone geometry and base positioning compared to canonical Watson–Crick base pairing (Fig. 1*C*), disrupting base stacking and thus helical stability (36). To confirm this, we measured melting temperature (T_m) values for each variant by ultraviolet (UV) thermal melting analyses under three conditions distinguished by low salt (10 mM NaCl), high salt (100 mM NaCl), and high salt with Mg^{2+} (100 mM NaCl, 7 mM $MgCl_2$). These conditions were selected as they reflect the components used in our OAS1 activation assay (i.e., 10 mM NaCl and 7 mM $MgCl_2$), but with Mg^{2+} included only in the presence of higher salt to reduce the potential for RNA hydrolysis by the divalent ion at higher temperatures. Under all three solution conditions, dsRNA T_m decreases as the number of inosine substitutions increases (Fig. 1*D*), consistent with the expected reduced dsRNA stability. Increasing solution ionic strength, that is, low salt vs. high salt and high salt vs. high salt with Mg^{2+}, shifts the T_m of each I•U base pair–containing dsRNA higher by similar amounts ($\Delta T_m \approx$ 10 °C to 12 °C) such that relative differences between the three dsRNAs remain the same regardless of the solution condition. The dsRNA T_m values in high salt (100 mM NaCl) therefore likely most closely reflect dsRNA stability under OAS1 in vitro assay conditions, and these are reported as average values in Table 1 for the IU variants and all other dsRNAs tested in subsequent experiments (individual measurements in all three conditions are also shown in *SI Appendix*, Table S1).

As a consequence of the reduced stability with I•U base pairs, we also expected to observe a corresponding strongly decreasing trend in each dsRNA's ability to activate OAS1. However, in an established in vitro OAS1 activation assay, the inosine-containing dsRNAs were all found to be well tolerated by OAS1 (Fig. 1*E* and Table 1). Further, this trend in modestly increasing OAS1 activation also directly correlated with the number of I•U base pairs incorporated (i.e., OAS1 activation order: AU3 < IU1 < IU2 < IU3). Thus, contrary to expectation, changes in the short dsRNA of the type arising from natural A-to-I editing do not decrease OAS1 activation, despite the anticipated reduction in dsRNA stability.

OAS1 Activation Is Enhanced by Inosine and Mismatches in the Center of Short dsRNAs. The ability of I•U pair–containing dsRNAs to modestly enhance OAS1 activation by the short dsRNA could arise through generally increased helical flexibility, specific change(s) in helical structure to accommodate the nonisosteric base pairs, or a particular property of the nonstandard inosine base itself. To begin addressing these possibilities, we generated two further series of 18-bp dsRNAs containing either I–C or A•C pairings with one, two, or three sets of substitutions at the same sites and with the same naming convention as before (Fig. 2 and *SI Appendix*, Fig. S1). These base pair substitutions were selected because I–C pairs place inosine in the same location as for the I•U pairs but maintain Watson–Crick-like base pairing and geometry, whereas A•C pairings introduce a different strongly destabilizing mismatch that does not contain inosine.

Table 1. Summary of short dsRNA stability and OAS1 activation

dsRNA	T_m (°C)*	Initial rate (nmol PP_i/min)†	Relative 28S rRNA cleavage‡
AU3	70.5	1.4 ± 0.1	1.0
IU1	66.8	1.8 ± 0.2	—
IU2	59.5	2.1 ± 0.3	—
IU3	54.5	2.6 ± 0.3	1.5 ± 0.3
IC1	69.3	1.9 ± 0.2	—
IC2	70.8	2.0 ± 0.2	—
IC3	71.0	2.4 ± 0.2	1.4 ± 0.3
AC1	64.8	2.3 ± 0.2	—
AC2	57.5	2.2 ± 0.2	—
AC3	49.3	3.0 ± 0.2	1.2 ± 0.1
GC1	72.3	1.7 ± 0.1	—
GC2	80.5	2.7 ± 0.2	—
GC3	84.0	2.8 ± 0.2	1.8 ± 0.4

*Melting temperature (T_m) in the high-salt (100 mM NaCl) condition; values are the average of at least two independent experiments. Individual values are shown in *SI Appendix*, Table S1.
†Initial rates of the reaction were determined for OAS1 activation assays by linear regression analysis on the first three or four time points of the reaction progress curve.
‡Quantification of the major 28S cleavage product (Fig. 6*B*, solid arrow) from three independent experiments in wild-type A549 cells. Values are normalized to AU3 dsRNA; —, not determined.

As expected, T_m values for the three I–C dsRNAs were similar to each other (within ~3 °C) under each given solution condition and also similar to AU3 dsRNA (Fig. 2*B*, Table 1, and *SI Appendix*, Table S1). Again, no specific differences in stability were observed between the low- and high-salt, or with Mg^{2+} conditions (*SI Appendix*, Table S1). Thus, unlike I•U pairs, I–C pairs do not destabilize the short dsRNA. Next, we assessed the three IC dsRNAs in the in vitro OAS1 activity assay and found that, despite their essentially identical stability, OAS1 activation was again modestly enhanced (Fig. 2*C* and Table 1). However, we note these base pair changes result in a different order of relative ability to activate OAS1 compared to the IU dsRNAs: Both IC1 and IC2 cause the same intermediate level of activation between AU3 and IC3, while three I–C pairs in IC3 most significantly increase OAS1 activity (i.e., order AU3 < IC1 ≈ IC2 < IC3).

Next, we tested the 18-bp dsRNA with one (AC1), two (AC2), or three (AC3) A•C mismatches (Fig. 2*D* and *SI Appendix*, Fig. S1) using the same two assays. As expected, a large shift to lower T_m was observed under all conditions as the number of A•C mismatches increases (Fig. 2*E*, Table 1, and *SI Appendix*, Table S1), with the same consistent T_m differences between conditions, albeit somewhat reduced for AC3 ($\Delta T_m \approx$ 6 °C on addition of Mg^{2+}; *SI Appendix*, Table S1). Remarkably, addition of A•C mismatches robustly enhanced OAS1 activation compared to AU3 dsRNA (Fig. 2*F*). Further, as for the I–C dsRNAs, all three A•C substitutions are required to achieve the largest enhancement in OAS1 activation, whereas AC1 and AC2 produced a similar intermediate level of OAS1 activity (i.e., order AU3 < AC1 ≈ AC2 < AC3).

Together, the results thus far show that base pair changes in the middle of the OAS1 consensus sequence that reduce helical stability (I•U and A•C base pairs) are unexpectedly well tolerated by OAS1. Further, inosine-containing dsRNAs are also

BIOCHEMISTRY

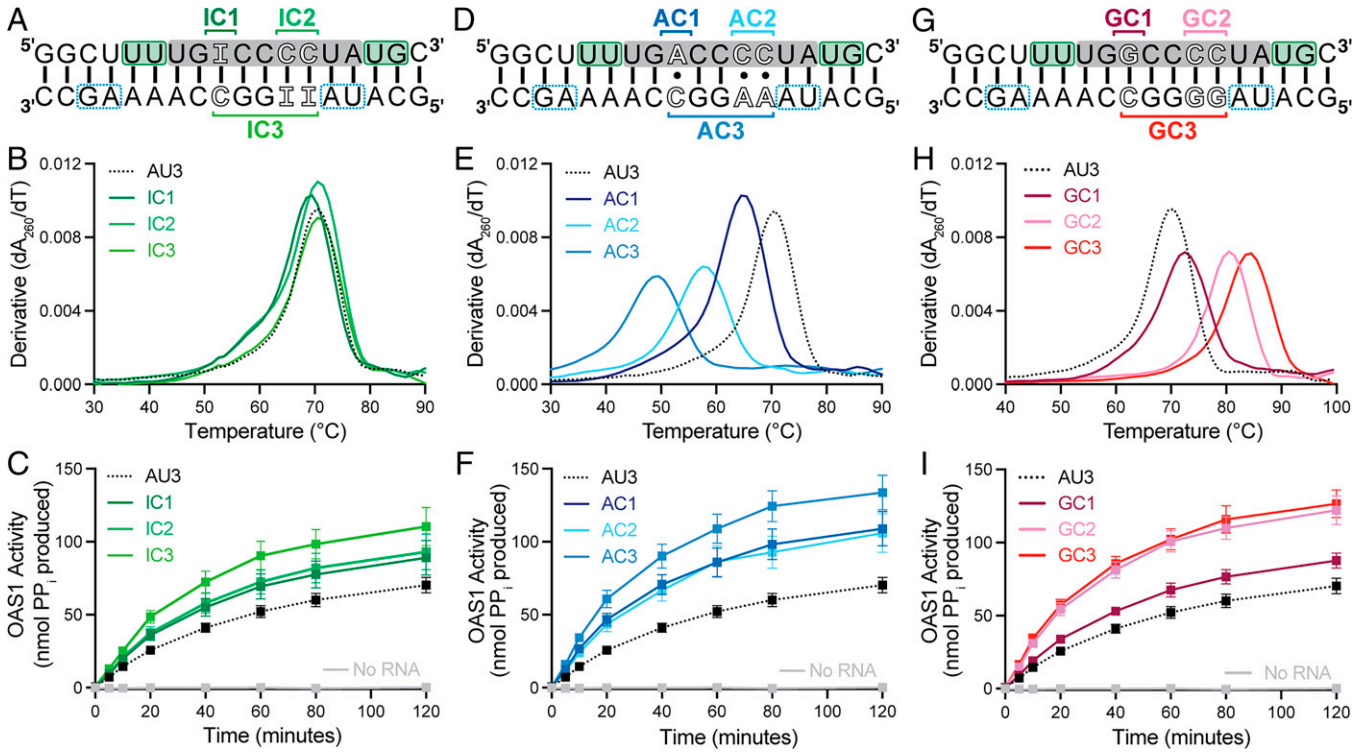

Fig. 2. OAS1 activation is increased by diverse base pair changes in the center of the 18-bp dsRNA. (*A*) Schematic of the 18-bp dsRNAs with one (IC1), two (IC2), or three (IC3) I–C base pairs. (*B*) UV thermal melting analysis of dsRNAs with I–C substitutions (green shades) and AU3 dsRNA (black dotted line) shown for comparison. (*C*) Reaction progress curves for in vitro OAS1 activation for all I–C variants and AU3 dsRNA. (*D–F*) and (*G–I*) Same as *A–C*, but for dsRNAs with A•C mismatches (blue shades) or G–C pairs (red shades), respectively, at the same locations.

modestly better activators regardless of whether the dsRNA is destabilized (I•U-containing dsRNAs) or not (I–C-containing dsRNAs). As noted earlier, OAS1-bound dsRNA adopts a distorted structure to make contacts with the protein via both ends of the RNA helix. Thus, destabilization of the dsRNA central region with I•U or A•C pairs could increase OAS1 activation by allowing this necessary helical structure to be more readily adopted. The potential for short dsRNA regions containing multiple destabilizing base pairings to activate OAS1 is particularly intriguing, as it suggests that searches for perfectly paired regions of >18 base pairs in cellular RNAs likely significantly underestimate the number of potential endogenous OAS1 activators. We therefore decided to further test this idea by examining dsRNAs with additional G–C base pairs which would be expected to have the opposite effect on helical stability.

Stabilization with G–C Substitutions Can Also Enhance OAS1 Activation by Short dsRNAs. As a first test of the idea that dsRNAs enriched in G–C base pairs would result in lower OAS1 activity due to increased helical stability or rigidity, we tested two high molecular weight homopolymers, poly(rA:rU) and poly(rG:rC), in comparison with the known potent OAS1 activator poly(rI:rC). Each homopolymer had widely different capacities to activate OAS1, with poly(rI:rC) dsRNA and poly(rG:rC) dsRNA (being the most and least potent, respectively; *SI Appendix*, Fig. S2*A*). The poly(rG:rC) dsRNA was found to only be capable of weakly activating at 60-fold higher concentration (*SI Appendix*, Fig. S2*B*). Thus, the results with long dsRNAs containing highly biased sequences support the idea that more stable and, likely, more rigid dsRNA is a poorer activator of OAS1. These results also underscore that poly(rI:rC) is an unusually potent OAS1 activator for reasons that are not currently apparent.

Next, to test whether addition of G–C base pairs has the same effect in the context of the 18-bp dsRNA, we generated dsRNAs with one (GC1), two (GC2), or three (GC3) G–C substitutions as before (Fig. 2*G* and *SI Appendix*, Fig. S1). As expected, UV thermal melting analysis revealed overall higher melting temperatures for all three GC variants compared to AU3, with a clear positive correlation between the number of G–C base pairs and the increase in T_m under all solution conditions (Fig. 2*H*, Table 1, and *SI Appendix*, Table S1). Surprisingly, however, the addition of G–C base pairs in the 18-bp dsRNA resulted in increased OAS1 activation (Fig. 2*I* and Table 1). In this set of dsRNAs, a further distinct pattern of relative activation was observed, with the tandem G–C substitutions of GC2 being sufficient to achieve the same highest level of activation as GC3 (i.e., order AU3 < GC1 < GC2 ≈ GC3). These results suggest there must be some other features, in addition to the destabilizing effects of the I•U and A•C pairs, that can lead to the observed increase in activation capacity.

Differences in dsRNA Structure Correlate with Their Capacity to Activate OAS1. Next, we used thermal difference spectra (TDS) to determine whether differences in dsRNA helical structure in each dsRNA variant series could be identified that might underpin the observed increases in OAS1 activity. TDS for nucleic acids are obtained by measuring UV absorbance spectra at two temperatures, one above and one below the T_m, corresponding to the unfolded and folded states of the molecule, respectively. The difference between these two spectra (the TDS) arises through changes in base stacking interactions and thus contains valuable information characteristic of a given nucleic acid structure (37).

The TDS spectrum for AU3 dsRNA is characterized by three major features: a broad positive peak at ~270 nm to 280 nm flanked by two minima; a broad, likely double, minimum at

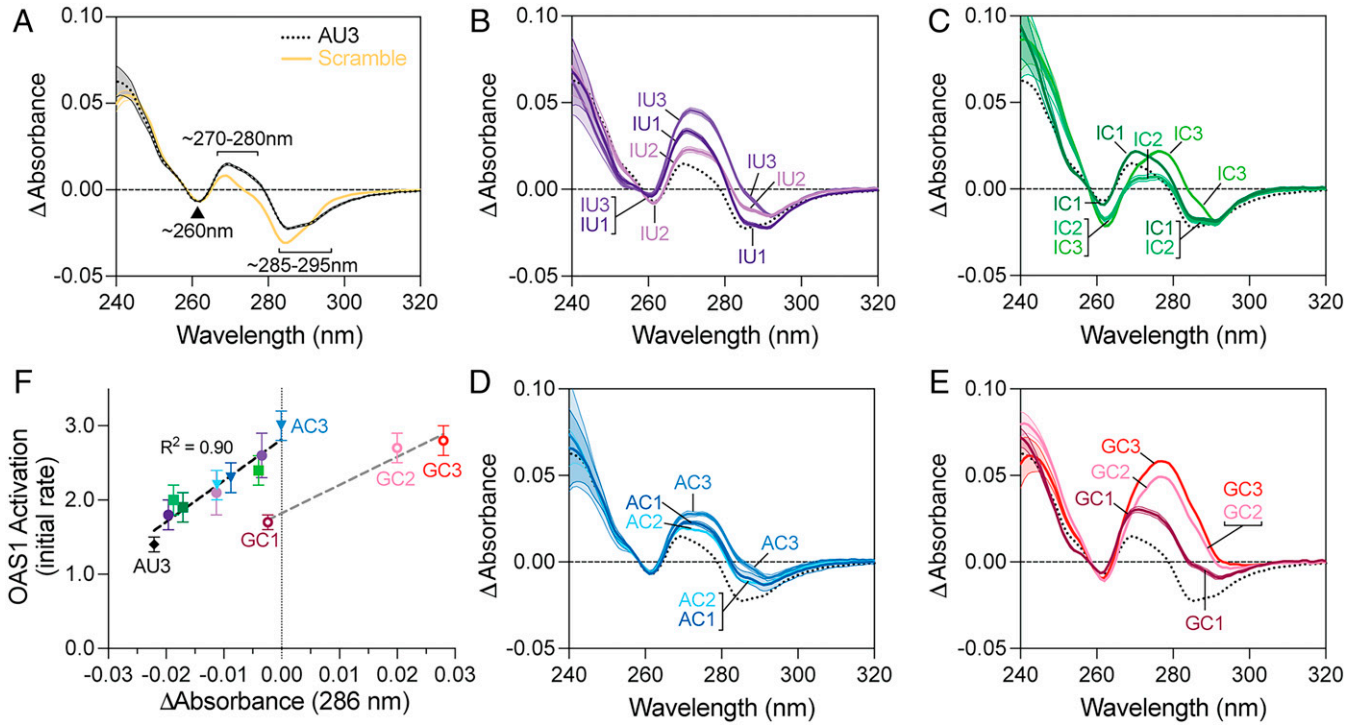

Fig. 3. TDS identify structural changes in dsRNA that correlate with OAS1 activation level. (*A*) TDS for AU3 and Scramble dsRNAs with characteristic regions indicated within the 240- to 320-nm wavelength range. (*B–E*) TDS for each dsRNA variant series with individual plots labeled at each spectral feature with changes compared to AU3 dsRNA (shown as black dotted line). All TDS plots are shown with SEM from three independent experiments as transparent shading on each curve. (*F*) Plot of TDS at 286 nm against initial rate of OAS1 activation for each dsRNA shows a strong positive correlation for this spectral feature.

~285 nm to 295 nm; and a weaker but sharper minimum at ~260 nm (Fig. 3*A*). Features below ~250 nm were more variable between replicate experiments (*SI Appendix*, Fig. S3) and were not considered further. A randomized sequence (Scramble) previously shown to lack any capacity to activate OAS1 (34) was also tested and exhibited clear differences in two of these regions (~270 nm to 280 nm and 285 nm to 295 nm; Fig. 3*A*). Similarly, differences in TDS spectra for each dsRNA variant series are observed compared to AU3 dsRNA, with common changes largely centered on an increase and/or rightward shift in the broad positive peak at ~270 nm to 280 nm and an increase (to a less negative value) in one or both components of the double negative peak at ~285 nm to 295 nm. Notably, the direction of these differences is opposite to that observed for the nonactivating Scramble dsRNA. Excellent correlation between these spectral changes and order of ability to activate OAS1 within each series is also observed, as discussed further below, indicating that the TDS differences reflect dsRNA base stacking and helical features relevant for OAS1 activation.

I•U pair–containing dsRNAs alter each of the three major TDS spectral features in specific ways (Fig. 3*B*). IU1 dramatically increases the broad ~270- to 280-nm peak and also slightly increases the negative peak at 260 nm, while the other negative peak at ~285 nm to 295 nm is essentially unaffected. In contrast, IU2 significantly increases the negative ~285- to 295-nm peak, but only more modestly increases the ~270- to 280-nm peak and has no effect at 260 nm. In IU3, these distinct effects are almost perfectly combined, with this dsRNA having the most pronounced increase at ~270 nm to 280 nm, the strongest increase in the negative peak at ~285 nm to 295 nm (particularly in the shorter wavelength half, ~285 nm to 290 nm), and an identical increase as observed for IU1 at 260 nm. Thus, these base pair changes and the base stacking and helical alterations they induce are consistent with in vitro OAS1 activation by these dsRNAs where IU1 and IU2 exhibit distinct intermediate levels of activation that are additive to make IU3 the most activating in this dsRNA series.

The I–C base pair changes also appear to impart unique differences in base stacking and helical structure. IC1 increases the positive ~270- to 280-nm peak but has essentially no effect on the other two regions. In contrast, IC2 sharply decreases (more negative) the 260-nm peak but also reduces the lower wavelength half of the positive ~270- to 280-nm peak (Fig. 3*C*). Finally, IC3 contains spectral features of both variants, including decreased 260-nm (IC2) and increased ~270- to 280-nm (IC1) peaks, but with pronounced rightward shift of the latter peak and loss of the shorter wavelength half of the negative ~285- to 290-nm peak. As for the IU dsRNAs, the changes in structure reflected in the TDS are consistent with the intermediate increase in OAS1 activation for IC1 and IC2 that combine in IC3 to make the strongest activator in this series of dsRNAs.

The dsRNAs with A•C base pairs each result in similar changes in TDS (Fig. 3*D*), with increases in both the positive ~270- to 280-nm and negative ~285- to 295-nm peaks (particularly in the shorter wavelength half, as for IU3). Here, AC1 and AC2 produce almost identical changes in the spectra, and these effects are additive in the spectrum for AC3. These results suggest that the A•C pairs induce similar, more global helical structure destabilization regardless of their location and, again, the changes in TDS accurately mirror the order of OAS1 activation: AC1 ≈ AC2 < AC3.

Finally, introduction of G–C base pairs results in the most pronounced changes in TDS of all the variant series, again centered on the peaks at ~270 nm to 280 nm and ~285 nm to 295 nm, with the negative 260-nm peak unaffected in all three dsRNAs (Fig. 3*E*). While GC1 induces an increase in both peaks, the changes for GC2 and GC3 dsRNA are more pronounced and also similar in magnitude. In both latter dsRNAs, the

negative ~285- to 295-nm peak is completely lost and appears, in part, as a shoulder on a broadened positive peak from ~270 nm to 290 nm. Thus, in contrast to the other dsRNA variants, for the G–C base pairs, there appears to be relatively little additive effect in changes caused by GC1 and GC2. Instead, the effect of the tandem G–C pair of GC2 appears to dominate in both GC2 and GC3 dsRNAs, again mirroring the order of activation: GC1 < GC2 ≈ GC3.

In summary, the TDS reveal that specific changes in base stacking and/or helical structure arise from the distinct base pair changes in each dsRNA variant series and that the nature and extent of these changes faithfully reflect the extent of OAS1 activation by each RNA. Further, many of these changes appear to be shared among several of the dsRNA variants. For example, change in TDS at 286 nm is highly correlated within and between the I•U, I–C, and A•C base pair–containing dsRNAs (Fig. 3*F*). At this wavelength, G–C base pair–containing dsRNAs also show an increase correlating with OAS1 activation (i.e., GC1 < GC2 ≈ GC3), but additional helical structure changes, that presumably do not impact OAS1 activation, result in significantly greater TDS. Together, these data clearly support the idea that dsRNA base stacking and helical structure, as dictated by multiple distinct sequence changes, play an important role in regulating the extent of OAS1 activation. While many changes observed in TDS are consistent between the most potent OAS1 activators in each dsRNAs variant series, the specific helical structures and/or dynamics underpinning these changes cannot be directly discerned. To gain such insights, we turned to MD simulations of these dsRNAs.

MD Simulation Reveals a Role for Helical Dynamics in OAS1 Activation. As noted earlier, a recent MD study identified alternating AU sequences of three or more consecutive nucleotides in length as a potential source of helical bending within dsRNA (35). We therefore first used one of the test sequences ("Seq3") from this study to benchmark our MD production protocol in the Desmond module of the Schrödinger software (release 2020-4). This benchmark analysis faithfully reproduced both the reported helical bending and narrowing of the major groove at the alternating AU sequence (*SI Appendix*, Fig. S4 *A* and *B*; details in *Materials and Methods*).

MD analysis was first performed for 200 ns for AU3 dsRNA and the variants with three base pair changes of each type (i.e., IU3, IC3, AC3, and GC3), as these dsRNAs showed the most pronounced changes in TDS correlated with enhanced OAS1 activation within each group of variants. Consistent with their decreased helical stability in the thermal melting studies, both IU3 and AC3 exhibited an overall higher rmsd compared to both AU3 and the other variants, IC3 and GC3 (*SI Appendix*, Fig. S4*C*). Greater flexibility in the structures of these two dsRNAs was also reflected by their significantly higher mean bending angle compared to the AU3, IC3, and GC3 dsRNAs (Fig. 4*A*). The IU3 and AC3 dsRNAs also showed an overall expanded range of bending angles and, for AC3, an overall upward shift of this expanded range to higher values. Consistent with higher overall rmsd and increase in helical bending, alignment of all 20 structures reveals larger variation in overall helical structure for both the IU3 and AC3 compared to AU3 dsRNA (Fig. 4*B*). In contrast, IC3 and, to an even greater extent, GC3 exhibit lower variation among the 20 representative structures.

Analysis of helical, base step, and base pair parameters using Curves+ (38, 39) reveals more detail on the wide-ranging impacts of these destabilizing base pair changes on dsRNA helical structure (*SI Appendix*, Fig. S5 *A–D*). Notably, however, in all cases, the first seven or eight base pairs or base pair steps, which comprise one region directly contacted by OAS1, are essentially indistinguishable from AU3 dsRNA. In IU3 and AC3 dsRNAs, large deviations in these structural parameters are centered on the regions following one or both of the sites with altered base pairs. As such, changes in helical and local base pair structure are localized to the central region between the conserved OAS1 consensus dinucleotides (WW/WG). With only one exception (for axial bend; *SI Appendix*, Fig. S5*A*), structural parameters for IU3 and AC3 dsRNAs return to values similar to AU3 dsRNA by the final two or three base pairs or base steps (*SI Appendix*, Fig. S5 *A–D*).

Examination of representative structures from the AC3 and IU3 simulations also reveals the potential for both tandem base pair substitutions (12:7′ and 13:6′, where ′denotes the bottom-strand nucleotide) to induce large local changes in helical structure and base stacking (Fig. 4 *C* and *D* and *SI Appendix*, Fig. S5*E*). Early in the IU3 simulation (within 30 ns to 50 ns), the U13:I6′ pair becomes disrupted, and U13 moves toward the helical axis, forming a hydrogen bond via its base N3 to the 2′-OH of I6′, creating a stack of three bases with the two inosines (I6′:U13:I7′; Fig. 4*C*). This structure subsequently persists throughout the simulation, with only one minor variation near the end of the simulation in which I6′ shifts up within the helical base stack nearer to A5′ (exemplified by the 200-ns representative structure in Fig. 4*C*). In contrast, the single I•U base pair (base pair 9:10′) maintains relatively consistent mismatched base pairing and base stacking interactions throughout the simulation (Fig. 4*D*). In AC3 dsRNA, we observe formation of a similar structure in which a purine base (A7′) rather than the pyrimidine shifts toward the central axis to form a similar single base stack (C13:A7′:C12; *SI Appendix*, Fig. S5*E*). While this structure persists over several 10-ns segments of the simulation, these changes in AC3 appear more transient, returning to structures with distinct tandem mismatch A•C pairs and, finally, second distinct nonhelical structure in which C13 is fully extruded from the helix (*SI Appendix*, Fig. S5), strongly kinking the RNA phosphodiester backbone.

In summary, the MD simulations reveal that inherent general deformability in the dsRNA region between the major contacts with OAS1 likely underpins the ability of the IU3 and AC3 dsRNA to more strongly drive allosteric activation of the enzyme. The potential formation of non–A-form helical structures, in particular by the tandem I•U pairs, may also have implications for the underlying mechanism by which editing masks cellular dsRNAs from other innate immune sensors (*Discussion*).

Stabilizing Base Pair Changes Can Predispose Short dsRNA Structure for OAS1 Activation. In contrast to AC3 and IU3 dsRNAs, the increased capacity of IC3 and, in particular, GC3 dsRNAs to activate OAS1 cannot result from a general increase in helical flexibility or deformability. To identify helical features that might contribute to increased OAS1 activation by stabilized dsRNAs, we ran additional simulations of GC1 (activation similar to AU3) and GC2 (activation similar to GC3). Both GC1 and GC2 dsRNAs exhibited similar rmsd and overall bending angle to AU3 dsRNA (Fig. 4*A* and *SI Appendix*, Fig. S4*C*, respectively). As before, helical and base pair/step parameters were determined using Curves+ (38, 39), but major differences were not immediately apparent (*SI Appendix*, Fig. S6 *A–D*). In particular, while some local base pair tilt values were identified that suggest GC2 and GC3 more closely mirror the OAS1-bound dsRNA structure than the less activating AU3 and GC1 dsRNAs (discussed further below), other parameters characteristic of local helical bending, such as major groove width and base pair roll, appear very similar in each of these dsRNAs. However, an important limitation in these comparisons is that all four RNAs have at least some capacity to activate OAS1. In contrast, MD simulation and comparison with the nonactivating Scramble dsRNA suggest that local helical structure is indeed

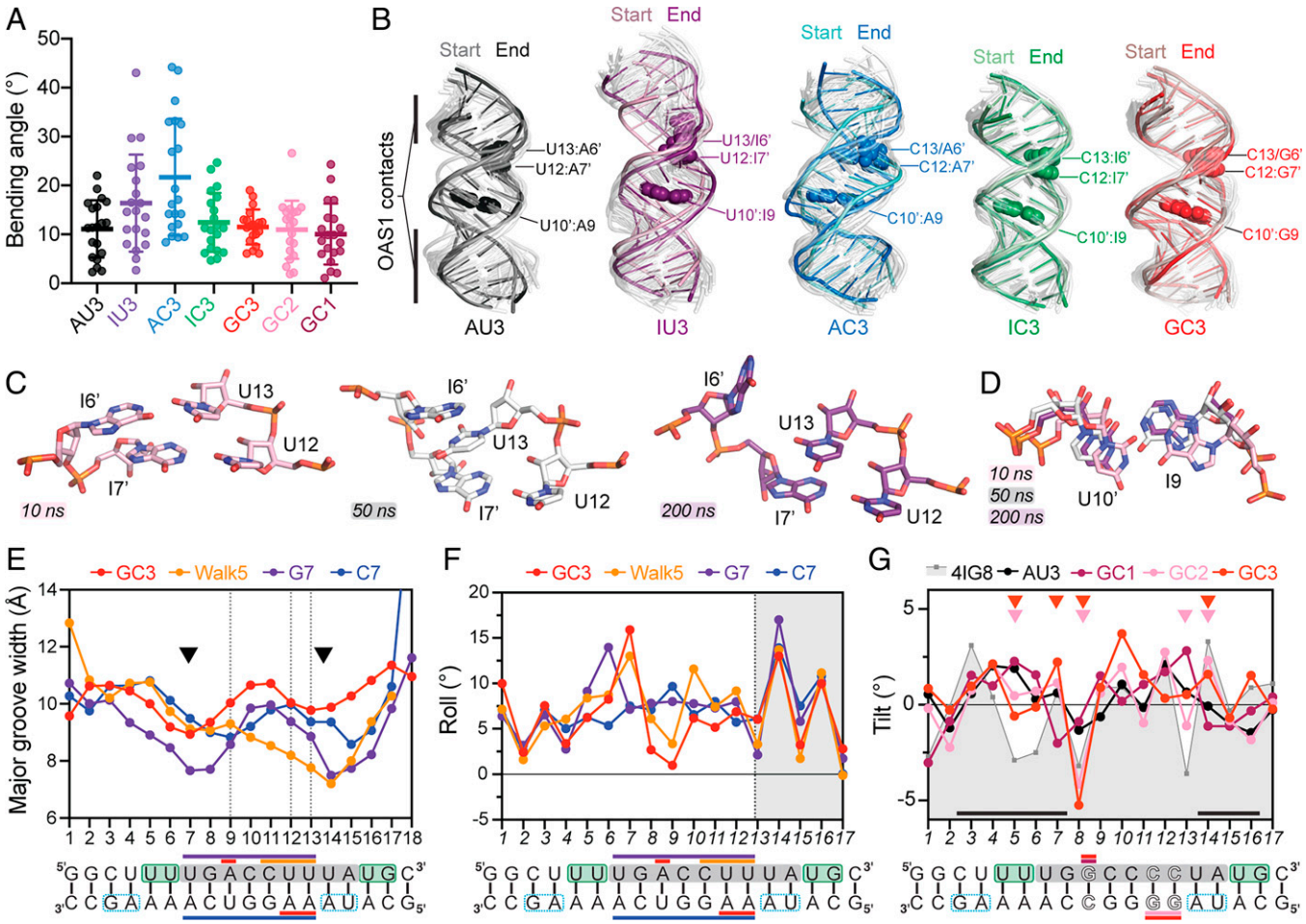

Fig. 4. Increased dsRNA dynamics and specific helical features underpin increased OAS1 activation by short dsRNAs. (*A*) Helical bending angle calculated for the 20 structures representative of each 10-ns segment of the 200-ns simulation for the indicated dsRNAs. (*B*) Alignment of all 20 representative structures for the indicated dsRNA highlighting the first (lighter color) and last (darker color) 10-ns segments of each simulation, with the 18 intermediate structures shown as semitransparent cartoons. The locations of altered base pairs in each dsRNA are noted, and the nucleobases are shown as spheres. (*C*) Interactions formed by the tandem I•U base pairs in representative structures at the indicated simulation times, colored as in *B*. (*D*) As in *C*, but for the single base pair change with the three structures overlaid. Results of helical analysis for (*E*) major groove width and (*F*) base pair roll for the most activating G/C-rich sequences: Walk5 (orange), G7 (purple), and C7 (blue), with GC3 (red) shown for reference. The locations of these substitutions are shown by color-coded bars on the dsRNA schematic below each plot (shown as AU3 dsRNA with the bar on the strand containing nucleotide changes. In *E*, arrowheads denote minima in the characteristic major groove profile of strong activators, and vertical dotted lines indicate the locations of base pair changes in GC3 dsRNA. In *F*, shading denotes roll in the region corresponding to the UAUG sequence. (*G*) Comparison of base pair tilt for the 20 representative structures from MD simulation of AU3 and the GC series dsRNAs (GC1, GC2, and GC3). Values for the OAS1-bound RNA structure (Protein Data Bank ID code 4IG8) are also indicated (gray shaded area). Steps with mean tilt values mirroring those in the bound dsRNA structure (4IG8) in the most activating GC2 and GC3 dsRNAs but not GC1 and AU3 are indicated above the plots with arrowheads. The black bar above the *x* axis indicates the main regions (on either strand) of contact with OAS1 in the complex crystal structure. The sequence of GC3 dsRNA is shown underneath for reference.

likely to be critical for OAS1 activation, particularly surrounding the consensus WG dinucleotide, where all three helical parameters strongly differ from the activating dsRNAs (*SI Appendix*, Fig. S6*E*).

To further explore the impact of G–C base pairs in the center of the short dsRNA, 11 additional dsRNAs were designed to determine whether some G/C-rich sequences might act as poorer OAS1 activators, as predicted by the experiments with poly(rG:rC). These new dsRNAs were thus also examined in an effort to resolve the apparent paradox that adding either destabilizing (I•U and A•C) or stabilizing (G–C) base pairs at the original sites in the N_9 sequence all led to better OAS1 activators. Applying the prior design constraints of maintaining the conserved WW/WG consensus dinucleotides on both strands, we generated three dsRNA series with systematic changes at the seven remaining variable internal positions (*SI Appendix*, Fig. S7*A*): 1) movement of a GC triplet sequence through the center of the dsRNA (Walk1 to Walk5), 2) increasing the number of G–C pairs (G4, G5, G6, and G7; all with G on the top strand), and 3) altering the organization of seven central G–C pairs [compare to G7: C7 with C on the top strand and $(CG)_3$ with alternating G/C bases on each strand]. As before, all 11 new dsRNAs were analyzed using MD simulations, and we first assessed correlations in roll angle, as characteristic changes in this parameter have previously been observed upon protein binding (40). Consistent with our dsRNA design constraints, the 11 new dsRNAs, as well as AU3 and GC3, exhibit high correlation within the conserved consensus and nonvarying termini nucleotides (*SI Appendix*, Fig. S7*B*, *Top*). In contrast, the non–OAS1-activating Scramble dsRNA shows largely anticorrelated roll values with all other dsRNAs. Further, among all dsRNAs, comparatively low correlation is observed in the central seven varying positions (*SI Appendix*, Fig. S7*B*, *Bottom*). Thus, by virtue of our dsRNA design strategy, some capacity to activate OAS1 is always enforced

by the consistent presence of the consensus and other nonvariable sequences, but the variable intervening helical structure may still confer enhanced, or potentially diminished, OAS1 activation due to its helical structure.

We next selected two dsRNAs from each series for OAS1 activation assays: Walk2 vs. Walk5, G5 vs. G7, and C7 vs. $(CG)_3$. Remarkably, in each pair, one dsRNA showed a further increased ability to activate OAS1 compared to GC3 dsRNA (Walk5, G7, and C7), while the other was either the same as the parent AU3 dsRNA (Walk2 and G5 dsRNAs; i.e., activity not enhanced by addition of G–C pairs) or poorer [$(CG)_3$ dsRNA; i.e., activity reduced by addition of G–C pairs] (*SI Appendix*, Fig. S7*C* and Table S2). Most strikingly, among the three sequences fully altered with seven G–C pairs, and thus identical base composition, are both the most (G7 and C7) and least [$(CG)_3$] activating dsRNAs identified thus far (*SI Appendix*, Fig. S7*C* and Table S2).

All analyzed dsRNAs, with the exception of the nonactivating Scramble, share a UAUG sequence due to the maintenance of top- and bottom-strand WWN_9WG consensus sequences (underlined nucleotides are the WG of the top-strand OAS1 consensus sequence). This sequence is located immediately adjacent to the site where the original tandem base pair changes were introduced to create GC2 and GC3 dsRNAs. Strikingly, the three additional G–C pair–containing constructs with increased capacity to activate OAS1 (Walk5, G7, and C7) all have their stabilizing sequences immediately adjacent to the UAUG sequence where a narrowing of the major groove is observed (*SI Appendix*, Fig. S7*D*), consistent with the reported effect of AU tract sequences on helical structure (35). This effect is most apparent for the strongest OAS1 activators which have a characteristic "W"-shaped major groove width profile, with narrowing at each end of the OAS1 consensus sequence (Fig. 4*E*). In contrast, two of the poorer activators, Walk2 and G5, have the stabilizing sequence placed distant from the UAUG sequence, separated by the tandem A–U pairs of the original dsRNA. Here, the major groove variation is flattened throughout their sequence, while the poorest activator combines flattening in the first half of the dsRNA with exaggerated variations through the $(CG)_3$ and UAUG sequences. In further support of an important role for this helical feature, Scramble dsRNA lacks the UAUG sequence and has a markedly widened major groove in this region (*SI Appendix*, Fig. S6*E*). Base pair roll is also highly correlated surrounding the UAUG sequence (base pair steps 13 to 17) among OAS1 activators (Fig. 4*F* and *SI Appendix*, Fig. S7*E*), but not Scramble dsRNA (*SI Appendix*, Fig. S6*E*). Thus, G–C base pair changes immediately preceding the UAUG sequence can stabilize a helical structure, characterized by distinct major groove shape and base pair roll, that predisposes the short dsRNA for optimal OAS1 interaction and thus increased capacity to activate OAS1.

We also note that local differences in other helical or base pair parameters could contribute to greater activation in subtle ways that are not entirely apparent from simulation of the free dsRNAs. For example, comparison of base pair tilt between GC2/GC3 and AU3 dsRNA reveals several sites where GC3 adopts a more OAS1-bound-like structure (Fig. 4*G*; regions marked with arrowheads). The majority of these sites (plus one additional adjacent site) are also present in the functionally (OAS1 activation) and structurally (TDS) most similar GC2 dsRNA, whereas GC1 dsRNA appears consistently more similar to AU3. As for the other parameters discussed above, Scramble dsRNA appears close to anticorrelated in tilt values throughout its sequence (*SI Appendix*, Fig. S6*E*).

Finally, as the impacts of I–C base pair introduction on 18-bp dsRNA helical structure and OAS1 activation were modest, we extended the MD studies in an effort to understand why poly(rI:rC) is such a potent activator of OAS1. Simulations of three additional dsRNAs were performed in which the central 18 base pairs were replaced with $(IC)_{18}$, $(AU)_{18}$, or $(GC)_{18}$ sequences. Several helical or base pair parameters were identified with significant differences in average values for the three sequences mirroring their relative abilities to activate OAS1, including X displacement, buckle, propeller, opening, and twist (*SI Appendix*, Fig. S8 *A–C*). While further detailed analyses are needed to identify the specific features of poly(rI:rC) responsible for its remarkable ability to activate OAS1, TDS analysis also confirms this dsRNA is structurally distinct from poly(rA:rU) (*SI Appendix*, Fig. S8*D*). Poly(rG:rC) dsRNA was too stable ($T_m \approx 105\,^{\circ}C$ in water) to allow determination of a TDS for additional comparisons with the most weakly activating long homopolymer. Poly(rI:rC) has a large negative TDS peak at 260 nm, the sole region that changed among the dsRNAs only for the tandem I–C pair–containing IC2 and IC3 dsRNAs, suggesting the same helical features contribute in each case, albeit much more modestly in the context of the short, mixed-sequence RNA.

OAS1-Activating Helical and Base Pair Features Are Additive. Our MD simulations revealed two distinct ways in which changes in the short dsRNA sequence can promote greater OAS1 activation: generally increased dynamics in the central region of the helix or local stabilization of helical structure. An obvious next question is whether these distinct effects can be combined in an additive manner in a single dsRNA to produce a more potent OAS1 activator. We therefore combined the AC1 and GC2 base pair changes (to make AC1–GC2 dsRNA; Fig. 5*A*) and did indeed find this dsRNA to be a better activator than either individual variant (Fig. 5*B*), with an initial rate of 4.7 ± 0.3 nmol PP_i/min (3.4-fold higher than AU3 dsRNA). TDS also revealed changes in characteristic peaks similar to those of GC2 dsRNA (Fig. 5*C*). Additionally, consistent with our interpretation of MD simulations thus far, AC1–GC2 dsRNA had both an increased overall rmsd compared to AU3 or any of the G–C pair–containing dsRNAs (*SI Appendix*, Fig. S4*C*) and an overall mean bending angle comparable to these dsRNAs (Fig. 5*D*). AC1–GC2 also exhibited characteristic global and local structural features in major groove width profile (Fig. 5*E*), as well as base pair roll and tilt (*SI Appendix*, Fig. S9 *A–C*). Similarly, combination of AC1 and GC2 base pair changes results in other helical and base pair parameters more like AU3 and the GC dsRNAs than AC3 (*SI Appendix*, Fig. S9 *D–F*), further underscoring the dominant effect of the tandem G–C pair on overall helical structure, enhanced by the presence of the flexibility conferring A•C pair.

Short dsRNAs Activate the OAS1/RNase L Pathway in Human Cells. To assess whether changes in short dsRNA structure and flexibility, and the enhanced OAS1 activation they impart in vitro, are relevant in a cellular context, we used an established assay of OAS1/RNase L pathway activation and subsequent rRNA degradation in human lung carcinoma A549 cells (Fig. 6*A*). Wild-type and RNase L knockout (KO) A549 cells were transfected with either AU3 or the dsRNA with three base pair changes from each dsRNA series, that is, IU3, IC3, AC3, or GC3, alongside mock transfection and poly(rI:rC) dsRNAs as negative and positive controls, respectively. Transfection of wild-type cells with each short dsRNA or poly(rI:rC) dsRNA resulted in degradation of 28S and 18S rRNA, consistent with pathway activation (Fig. 6*B*, *Top*). In contrast, no rRNA cleavage was observed in the RNase L KO cells despite a similar level of OAS1 expression (Fig. 6 *B* and *C*), confirming that dsRNA-induced cleavage is a direct consequence of OAS/RNase L pathway activation. The extent of rRNA cleavage among the short dsRNAs was assessed by quantifying the major 28S cleavage product (Fig. 6*B*, solid arrow) relative to AU3 dsRNA (Fig. 6*D* and Table 1), and the respective capacity of each dsRNA was found to follow a trend similar to in vitro OAS1 activation, with the exception of AC3 dsRNA (Fig. 6*D*). As we have

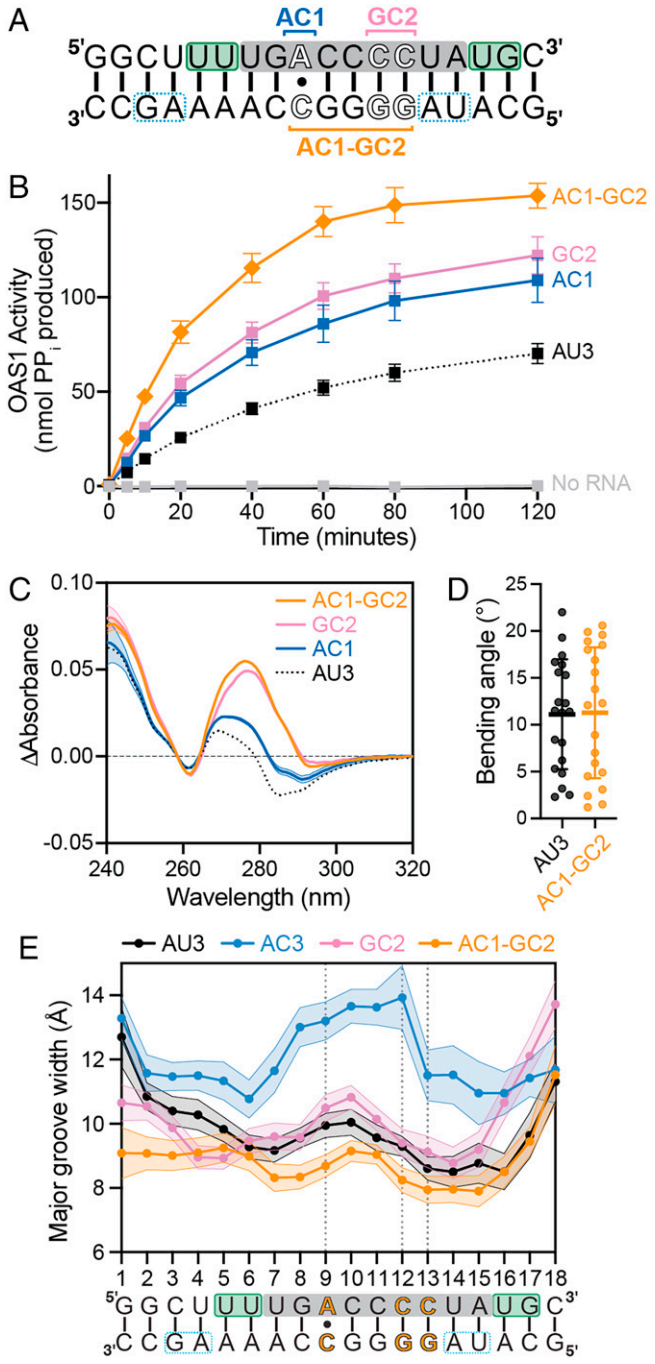

Fig. 5. Sequence changes resulting in increased OAS1 activation via distinct molecular mechanisms are additive. (*A*) Schematic of the 18-bp dsRNA AC1–GC2 combining the AC1 and GC2 base pair changes. (*B*) Reaction progress curves from an in vitro chromogenic assay of OAS1 activity using a single dsRNA concentration (300 nM) showing OAS1 activation is enhanced by combination of the AC1 and GC2 base pair changes in AC1–GC2 dsRNA. Data for AU3, AC1, and GC2 dsRNAs shown for comparison are the same as in Fig. 2. (*C*) Comparison of TDS for AC1–GC2 with individual AC1, GC2, and AU3 dsRNAs (same spectra as in Fig. 3). All TDS plots (except AU3) are shown with SEM from three independent experiments as transparent shading on each curve. (*D*) Helical bending angle calculated for the 20 structures representative of each 10-ns segment of the 200-ns simulation of AC1–GC2 dsRNA. Data for AU3 shown for comparison are the same as in Fig. 4. (*E*) Comparison of major groove width for the 20 representative structures of AC1–GC2 dsRNA and other indicated dsRNAs. The sequence of AC1–GC2 dsRNA is shown underneath for reference and vertical dotted lines indicate the locations of base pair changes.

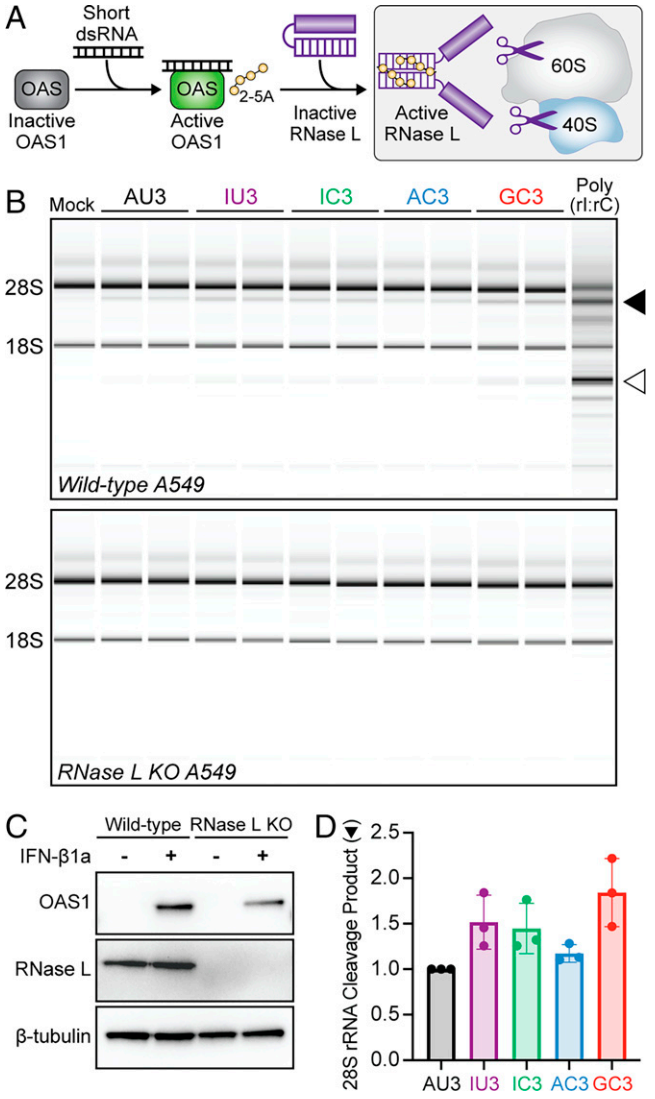

Fig. 6. Short dsRNA variants activate the OAS1/RNase L pathway in human cells. (*A*) Schematic of OAS1/RNase L pathway activation: dsRNA binding activates 2-5A synthesis by OAS1 and thus dimerization and activation of RNase L and subsequent cleavage of 28S and 18S rRNAs at specific sites. (*B*) Analysis of rRNA integrity in wild-type (*Top*) or RNase L KO (*Bottom*) A549 cells following transfection with dsRNAs: AU3 (black), IU3 (purple), IC3 (green), AC3 (blue), and GC3 (red). Mock transfection and transfection with poly(rI:rC) dsRNA serve as negative and positive controls, respectively. The 28S/18S rRNA degradation (arrows) is indicative of OAS1/RNase L pathway activation. A representative experiment with technical duplicates for each dsRNA is shown. (*C*) Western blot analysis confirming both OAS1 expression following IFN-β1a treatment and absence of RNase L in the RNase L KO cells. (*D*) Quantification of the 28S rRNA cleavage product (*B*, solid arrow) for each dsRNA normalized to cleavage induced by AU3 (*black*). Data are shown as the mean with SD for three independent experiments.

previously observed strong congruence between in vitro and cellular OAS1 activation (33, 34), the discrepancy observed for AC3 dsRNA could be due to lower transfection efficiency and/or the multiple mismatched base pairs rendering this short dsRNA more susceptible to strand dissociation and degradation by cellular RNases. It is also important to note that the short dsRNAs are the minimal length (~18 bp) required to activate OAS1 and are too short to activate OAS2 and OAS3; therefore, the greater observed rRNA cleavage for poly(rI:rC) dsRNA is likely due to both its potency as an activator of OAS1 and its ability to activate additional OAS family members.

Discussion

Prompted by a recent report that A-to-I editing by ADAR1 is responsible for limiting inadvertent activation of the OAS/RNase L pathway by endogenous dsRNAs (29), we first set out to determine OAS1 sensitivity to inosine modifications within a short 18-bp dsRNA. Surprisingly, both in vitro and cell-based assays of OAS1 activation revealed that not only were these inosine base pair–containing dsRNAs well tolerated by OAS1, but we observed small increases in activity correlating with the number of sequence changes incorporated. Short dsRNAs adopt a bent, imperfect A-form helix when bound to OAS1, allowing interactions with the protein at two locations on its surface (1, 2). Thus, sequence changes that alter dsRNA structure or dynamics, making the helix either too flexible or too rigid, were expected to alter the short dsRNA's ability to regulate OAS1 activation. Remarkably, however, in addition to the inosine base pair–containing dsRNAs, dsRNAs with either destabilizing A•C mismatches or specifically placed stabilizing G–C base pairs all showed enhanced ability to activate OAS1. Subsequent TDS analyses and MD simulations identified both local and global changes in dsRNA shape and flexibility that correlate with their respective impacts on OAS1 activation. Thus, we showed that dsRNA structure and predisposition to adopting a more OAS1-bound-like conformation are important considerations for OAS1 activation by dsRNA.

Our analysis of short dsRNAs with different base pair changes revealed TDS to be highly sensitive to altered base stacking and revealed unique structural fingerprints corresponding to changes in dsRNA helical structure which precisely mirrored the trends observed in OAS1 activation in vitro. To date, TDS has been used in a limited fashion for analyses of small DNAs, providing useful comparative fingerprints for distinct DNA structures (37). However, very little is known regarding the origin of specific bands in these spectra, particularly in the case of RNA molecules, limiting detailed interpretation of spectral changes. However, we speculate that altered within-strand purine–purine stacking may be a possible origin for some TDS changes we observed to correlate well with OAS1 activation (e.g., at 286 nm), given the sequence context of the base pair changes in our dsRNAs (*SI Appendix*, Fig. S1*D*). Clearly, however, our analyses of these short dsRNAs with relatively small sequence alterations reveal TDS to be unexpectedly rich in information. As such, further studies are warranted to define the origins of TDS features to enhance the utility of this technique in the analysis of dsRNA helical structures and their impact on RNA–protein interactions.

In the absence of infection, A-to-I editing of cellular RNAs by ADAR1 was proposed to be a protective measure to prevent aberrant activation of the OAS/RNase L pathway. This posttranscriptional modification alters base pair geometry and decreases RNA stability such that A-to-I editing may remove double-stranded regions required for OAS protein activation. However, contrary to this expectation, for OAS1, inosine-containing pairs or changes that otherwise disrupt the RNA helical structure were found to inversely correlate with enzyme activation. MD simulations demonstrated that IU3 and AC3 dsRNAs undergo greater changes in dsRNA structure and flexibility, allowing them to more readily adopt a bent conformation, required for OAS1 recognition, while not disrupting direct contacts made between OAS1 and the conserved consensus sequence dinucleotides (WW/WG) located on each end of the dsRNA helix. We note that OAS1's tolerance for inosine modification appears contradictory to previous findings that ADAR1 is responsible for suppressing aberrant activation of RNase L (29). However, it has not been determined which OAS protein(s) are specifically responsible for pathway activation in the absence of ADAR1 activity. We speculate that OAS3 may be predominant in the ADAR1-deficient context, and it may be that the extended helical structure and stability of longer dsRNAs that are required for its activation (>50 bp) are more significantly impacted by inosine modification. Alternatively, with its multidomain architecture, OAS3 may be less able to tolerate increased helical flexibility than we find OAS1 to be. Thus, building on the current work, further studies with other OAS proteins could delineate distinct sensitivities to inosine modification among OAS family members and the breadth of the protective mechanism conferred by ADAR activity against self-dsRNA activation.

The MD simulations also suggested a potential for tandem mismatches (I•U or A•C) to form irregular "zipper-like" structures within the dsRNA helix. Such structures in the tandem mismatch may be dependent on their combination with additional destabilizing mismatch(es), as they were observed for both AC3 and IU3 dsRNA as well as a replicate IU3 simulation, but not simulation of IU2 dsRNA. Whether such structures form within dsRNAs and the necessary contexts such as sequence (e.g., II/UU vs. IU/UI) or proximity of other mismatches will require further MD and experimental studies. However, we note that the resulting major distortions of the A-form helix identified here offer an alternative mechanism beyond simple destabilization for how A-to-I editing masks cellular dsRNA regions from innate immune sensors whose activity is highly dependent on A-form helical geometries such as PKR (41) or RIG-I (42).

The long poly(rG:rC) dsRNA was found to be an exceptionally poor OAS1 activator, consistent with the idea that forming a more rigid dsRNA should dampen OAS1's ability to sense these dsRNAs. However, in the context of the short dsRNA, additional G–C base pairs within the consensus N_9 region, at the same sites as used to increase flexibility with I•U and A•C pairs, unexpectedly resulted in a substantial increase in OAS1 activation. This finding thus resulted in the apparent paradox that both destabilizing and stabilizing base pair changes at the same sites in the center of the dsRNA can have similar impacts on OAS1 activation. Additional dsRNAs with systematic variations of G–C base pair content and position within the dsRNA were thus used to identify additional strongly activating sequences as well as the expected poorer activators. RNA helical analyses revealed that enhanced OAS1 activation required placement of the stabilizing G–C base pairs immediately adjacent to an UAUG sequence (underlined nucleotides are the conserved WG of the OAS1 consensus sequence) shared by all sequences other than the non–OAS1-activating Scramble dsRNA. Consistent with the reported effect of AU tract sequences on helical structure (35), these dsRNAs with correct placement of stabilizing G–C base pairs exhibited characteristic narrowing of the major groove at each end of the central region of the dsRNA. We also propose that this placement of G–C base pairs immediately prior to the conserved consensus sequence WG stabilizes helical features (e.g., base pair roll and tilt) in a manner that structurally predisposes the dsRNA for OAS1 activation. By reducing the need for OAS1 binding to induce required conformational changes in the dsRNA, these local helical structures may thus lead to the increased OAS1 activation we observed both in vitro and in A549 cells. Thus, in the case of dsRNAs that are inherently more dynamic, effects appear to be additive, as increasing flexibility allows the dsRNA to more readily adopt the necessary distorted bound conformation, while dsRNAs that are appropriately stabilized in a location-specific manner act by enhancing the effect(s) of other OAS1-activating features.

In summary, this work has revealed an unexpected tolerance in OAS1 for inosine-containing base pairs or other destabilizing mismatches, and significantly greater than previously appreciated complexity in the WWN_9WG OAS1 activation consensus sequence. In particular, dsRNA helical dynamics (flexibility) or stabilization of specific helical structural features are dictated by the N_9 sequence and are thus critical features for promoting optimal OAS1 activation. Although the differences between the dsRNA

are relatively small (up to approximately fourfold), sustained activation at such elevated levels during infection would promote significantly faster accumulation of sufficient 2-5A to effect a more rapid cellular response and earlier amplification of downstream antiviral activities. Further, recent evidence shows that even very low levels of persistent 2-5A synthesis from OAS1 gain-of-function activity can have dramatic cellular consequences and lead to devastating human disease (43). Our insights also provide a basis for better understanding how more complex, structured RNAs may accomplish their strong OAS1 activation. More importantly, these data also greatly expand the potential sequences (of either viral or cellular origin) capable of OAS1 activation with the tolerance of, or even preference for, mismatched bases.

Materials and Methods

Sample Preparation and OAS1 Activity Assays. All procedures for OAS1 expression in *Escherichia coli*, protein purification, generation of dsRNAs from individual chemically synthesized RNA oligonucleotides, and in vitro and cell-based OAS1 activation assays were performed essentially as described previously (32–34, 44). These procedures and those for RNA thermal melting analysis, generation of homopolymer dsRNAs, and immunoblotting are also described in more detail in *SI Appendix*.

TDS. Absorbance spectra (225 nm to 340 nm) were collected with a scan speed of 3,000 nm/min and a data interval of 1 nm on a Cary 3500 UV-Vis spectrophotometer (Agilent) at two temperatures, one above (95 °C) and one below (20 °C) the T_m of all dsRNAs under study. Samples contained ∼25 μg of RNA in a solution of 25 mM 3-(*N*-morpholno)propanesulfonic acid (pH 7.4) containing 10 mM NaCl, 7 mM $MgCl_2$, and 0.1 mM ethylenediaminetetraacetic acid. Individual spectra were normalized and difference spectra obtained by subtracting the low-temperature spectrum from the high-temperature spectrum (*SI Appendix*, Fig. S3*A*). Final plots were cut at 240 nm due to variability at shorter wavelengths (225 nm to 240 nm; *SI Appendix*, Fig. S3*B*) despite minimal variability between dsRNA preparations (*SI Appendix*, Fig. S3*C*). Three independent experiments were plotted with SEM using GraphPad Prism 9.

dsRNA MD Simulations. Before performing MD analysis of the 18-bp dsRNAs, a previously reported dsRNA sequence ["Seq3" (35)] was used as a benchmark for our MD protocol (details in *SI Appendix*). MD simulations were performed on select dsRNA sequences after addition of short terminal sequences of four G–C base pairs (GGGG/CCCC; "G4") to give computational constructs in the form of G4–X–G4, where X = AU3, IU3, IC3, AC3, GC3, GC2, or GC1 dsRNAs. This design was used to prevent end fraying or other improper conformational changes during the MD production run at the helix ends from impacting our analysis of each 18-bp sequence. One additional dsRNA from our prior study (34) (X = "Scramble"), a series of systematically designed G/C-rich dsRNAs (*SI Appendix*, Fig. S7*A*), and three dsRNAs with highly biased sequences (X = $(AU)_{18}$, $(GC)_{18}$, $(IC)_{18}$) were also analyzed in the same way.

The dsRNA structures were built using the biopolymer building panel, and MD simulation was performed in Desmond using the OPLS3e force field of the Schrödinger software (2020-4; Schrödinger). Each system was first neutralized by adding Na^+ around the dsRNA using the System Builder module. The neutralized dsRNA was then placed in TIP3P water, and random water molecules were substituted with Na^+ in order to obtain a total ionic strength of 10 mM NaCl. The solvated system was relaxed using a series of minimization stages, each of 1-ns duration, with all heavy atoms of the RNA restrained with force constant 1) 100, 2) 25, and 3) 5 kcal/mol$Å^2$ and, finally, 4) with no constraints. Each dsRNA system was heated to 300 K and equilibrated in the isobaric–isothermal (NPT) ensemble ($P = 1$ atm, $T = 300$ K) for 20 ns. Production simulations were then performed in the canonical (NVT) ensemble using the last configuration of the NPT equilibration for a 200-ns production run. For unrestrained MD simulations, Langevin thermostat and barostat were used with relaxation times of 1 and 2 ps, respectively. The equations of motion were integrated using multiple time steps for short-range (2 fs) and long-range (6 fs) interactions, with a 9-Å cutoff applied for nonbonded interactions. Coordinates were saved every 100 ps.

Representative structures in each 10-ns window (100 frames) over the 200-ns run were selected by using the Schrödinger software to determine the closest structure to the average of all structures within each window based on rmsd and low energy. The resulting 20 structures for each dsRNA were analyzed for helical bending, intrabase and interbase pair parameters, and groove dimensions using Curves+ (38, 39) after removal of the G4 cap regions from each of the dsRNAs, where applicable. Plots of rmsd (Schrödinger software) and dsRNA helical parameters (Curves+) were generated in GraphPad Prism 9.

Data Availability. All study data are included in the article and/or *SI Appendix*.

ACKNOWLEDGMENTS. We thank Dr. Susan Weiss (University of Pennsylvania School of Medicine) for generously providing RNase L KO and associated parental A549 cells. We also thank Drs. Christine M. Dunham, Richard A. Kahn, and Daniel Reines for discussion and comments on the manuscript. This work was supported by NIH Awards R01-AI144067 (to G.L.C.) and T32-GM008367 and F31-AI133950 (to S.L.S.). S.L.S. also gratefully acknowledges support from the Atlanta Chapter of The Achievement Rewards for College Scientists (ARCS) Foundation.

1. J. Donovan, M. Dufner, A. Korennykh, Structural basis for cytosolic double-stranded RNA surveillance by human oligoadenylate synthetase 1. *Proc. Natl. Acad. Sci. U.S.A.* **110**, 1652–1657 (2013).
2. J. Lohofener *et al.*, The activation mechanism of 2′-5′-oligoadenylate synthetase gives new insights into OAS/cGAS triggers of innate immunity. *Structure* **23**, 851–862 (2015).
3. B. Dong *et al.*, Intrinsic molecular activities of the interferon-induced 2-5A-dependent RNase. *J. Biol. Chem.* **269**, 14153–14158 (1994).
4. Y. Han, G. Whitney, J. Donovan, A. Korennykh, Innate immune messenger 2-5A tethers human RNase L into active high-order complexes. *Cell Rep.* **2**, 902–913 (2012).
5. H. Huang *et al.*, Dimeric structure of pseudokinase RNase L bound to 2-5A reveals a basis for interferon-induced antiviral activity. *Mol. Cell* **53**, 221–234 (2014).
6. W. Al-Ahmadi, L. Al-Haj, F. A. Al-Mohanna, R. H. Silverman, K. S. Khabar, RNase L downmodulation of the RNA-binding protein, HuR, and cellular growth. *Oncogene* **28**, 1782–1791 (2009).
7. O. Fabre *et al.*, RNase L controls terminal adipocyte differentiation, lipids storage and insulin sensitivity via CHOP10 mRNA regulation. *Cell Death Differ.* **19**, 1470–1481 (2012).
8. S. E. Brennan-Laun *et al.*, RNase L attenuates mitogen-stimulated gene expression via transcriptional and post-transcriptional mechanisms to limit the proliferative response. *J. Biol. Chem.* **289**, 33629–33643 (2014).
9. S. Banerjee *et al.*, RNase L is a negative regulator of cell migration. *Oncotarget* **6**, 44360–44372 (2015).
10. S. Rath *et al.*, Human RNase L tunes gene expression by selectively destabilizing the microRNA-regulated transcriptome. *Proc. Natl. Acad. Sci. U.S.A.* **112**, 15916–15921 (2015).
11. S. N. Sarkar, A. Ghosh, H. W. Wang, S. S. Sung, G. C. Sen, The nature of the catalytic domain of 2′-5′-oligoadenylate synthetases. *J. Biol. Chem.* **274**, 25535–25542 (1999).
12. M. S. Ibsen *et al.*, The 2′-5′-oligoadenylate synthetase 3 enzyme potently synthesizes the 2′-5′-oligoadenylates required for RNase L activation. *J. Virol.* **88**, 14222–14231 (2014).
13. J. Donovan, G. Whitney, S. Rath, A. Korennykh, Structural mechanism of sensing long dsRNA via a noncatalytic domain in human oligoadenylate synthetase 3. *Proc. Natl. Acad. Sci. U.S.A.* **112**, 3949–3954 (2015).
14. Y. Wang, A. Holleufer, H. H. Gad, R. Hartmann, Length dependent activation of OAS proteins by dsRNA. *Cytokine* **126**, 154867 (2019).
15. S. Wu *et al.*, 2′-5′-Oligoadenylate synthetase 1 polymorphisms are associated with tuberculosis: A case-control study. *BMC Pulm. Med.* **18**, 180 (2018).
16. G. Leisching, V. Cole, A. T. Ali, B. Baker, OAS1, OAS2 and OAS3 restrict intracellular M. tb replication and enhance cytokine secretion. *Int. J. Infect. Dis.* **80S**, S77–S84 (2019).
17. H. J. Lee *et al.*, Integrated pathogen load and dual transcriptome analysis of systemic host-pathogen interactions in severe malaria. *Sci. Transl. Med.* **10**, eaar3619 (2018).
18. L. L. Field *et al.*, OAS1 splice site polymorphism controlling antiviral enzyme activity influences susceptibility to type 1 diabetes. *Diabetes* **54**, 1588–1591 (2005).
19. M. Fedetz *et al.*, OAS1 gene haplotype confers susceptibility to multiple sclerosis. *Tissue Antigens* **68**, 446–449 (2006).
20. X. Feng *et al.*, Association of increased interferon-inducible gene expression with disease activity and lupus nephritis in patients with systemic lupus erythematosus. *Arthritis Rheumatol.* **54**, 2951–2962 (2006).
21. H. Li *et al.*, Identification of a Sjogren's syndrome susceptibility locus at OAS1 that influences isoform switching, protein expression, and responsiveness to type I interferons. *PLoS Genet.* **13**, e1006820 (2017).
22. S. Mandal, F. Abebe, J. Chaudhary, 2′-5′ oligoadenylate synthetase 1 polymorphism is associated with prostate cancer. *Cancer* **117**, 5509–5518 (2011).
23. A. A. Dar *et al.*, Extracellular 2′5′-oligoadenylate synthetase 2 mediates T-cell receptor CD3-zeta chain down-regulation via caspase-3 activation in oral cancer. *Immunology* **147**, 251–264 (2016).
24. C. Yu *et al.*, Prediction of key genes and pathways involved in trastuzumab-resistant gastric cancer. *World J. Surg. Oncol.* **16**, 174 (2018).
25. M. M. Lamers, B. G. van den Hoogen, B. L. Haagmans, ADAR1: "Editor-in-chief" of cytoplasmic innate immunity. *Front. Immunol.* **10**, 1763 (2019).
26. C. E. Samuel, Adenosine deaminase acting on RNA (ADAR1), a suppressor of double-stranded RNA-triggered innate immune responses. *J. Biol. Chem.* **294**, 1710–1720 (2019).
27. J. Quin *et al.*, ADAR RNA modifications, the epitranscriptome and innate immunity. *Trends Biochem. Sci.* **46**, 758–771 (2021).

28. G. I. Rice *et al.*, Mutations in ADAR1 cause Aicardi-Goutières syndrome associated with a type I interferon signature. *Nat. Genet.* **44**, 1243–1248 (2012).
29. Y. Li *et al.*, Ribonuclease L mediates the cell-lethal phenotype of double-stranded RNA editing enzyme ADAR1 deficiency in a human cell line. *eLife* **6**, e25687 (2017).
30. R. Hartmann *et al.*, Activation of 2′-5′ oligoadenylate synthetase by single-stranded and double-stranded RNA aptamers. *J. Biol. Chem.* **273**, 3236–3246 (1998).
31. R. Kodym, E. Kodym, M. D. Story, 2′-5′-Oligoadenylate synthetase is activated by a specific RNA sequence motif. *Biochem. Biophys. Res. Commun.* **388**, 317–322 (2009).
32. V. K. Vachon, B. M. Calderon, G. L. Conn, A novel RNA molecular signature for activation of 2′-5′ oligoadenylate synthetase-1. *Nucleic Acids Res.* **43**, 544–552 (2015).
33. B. M. Calderon, G. L. Conn, A human cellular noncoding RNA activates the antiviral protein 2′-5′-oligoadenylate synthetase 1. *J. Biol. Chem.* **293**, 16115–16124 (2018).
34. S. L. Schwartz *et al.*, Human OAS1 activation is highly dependent on both RNA sequence and context of activating RNA motifs. *Nucleic Acids Res.* **48**, 7520–7531 (2020).
35. A. Marin-Gonzalez *et al.*, Double-stranded RNA bending by AU-tract sequences. *Nucleic Acids Res.* **48**, 12917–12928 (2020).
36. M. J. Serra, P. E. Smolter, E. Westhof, Pronounced instability of tandem IU base pairs in RNA. *Nucleic Acids Res.* **32**, 1824–1828 (2004).
37. J. L. Mergny, J. Li, L. Lacroix, S. Amrane, J. B. Chaires, Thermal difference spectra: A specific signature for nucleic acid structures. *Nucleic Acids Res.* **33**, e138 (2005).
38. R. Lavery, M. Moakher, J. H. Maddocks, D. Petkeviciute, K. Zakrzewska, Conformational analysis of nucleic acids revisited: Curves+. *Nucleic Acids Res.* **37**, 5917–5929 (2009).
39. C. Blanchet, M. Pasi, K. Zakrzewska, R. Lavery, CURVES+ web server for analyzing and visualizing the helical, backbone and groove parameters of nucleic acid structures. *Nucleic Acids Res.* **39**, W68–W73 (2011).
40. C. A. Bewley, A. M. Gronenborn, G. M. Clore, Minor groove-binding architectural proteins: Structure, function, and DNA recognition. *Annu. Rev. Biophys. Biomol. Struct.* **27**, 105–131 (1998).
41. P. C. Bevilacqua, T. R. Cech, Minor-groove recognition of double-stranded RNA by the double-stranded RNA-binding domain from the RNA-activated protein kinase PKR. *Biochemistry* **35**, 9983–9994 (1996).
42. S. C. Devarkar, B. Schweibenz, C. Wang, J. Marcotrigiano, S. S. Patel, RIG-I uses an ATPase-powered translocation-throttling mechanism for kinetic proofreading of RNAs and oligomerization. *Mol. Cell* **72**, 355–368.e4 (2018).
43. T. Magg *et al.*, Heterozygous OAS1 gain-of-function variants cause an autoinflammatory immunodeficiency. *Sci. Immunol.* **6**, eabf9564 (2021).
44. J. Justesen, N. O. Kjeldgaard, Spectrophotometric pyrophosphate assay of 2′,5′-oligoadenylate synthetase. *Anal. Biochem.* **207**, 90–93 (1992).